

Numerical Heat Transfer, Part B: Fundamentals

An International Journal of Computation and Methodology

ISSN: 1040-7790 (Print) 1521-0626 (Online) Journal homepage: <https://www.tandfonline.com/loi/unhb20>

Analysis of the operator splitting scheme for the Allen–Cahn equation

Zhifeng Weng & Longkun Tang

To cite this article: Zhifeng Weng & Longkun Tang (2016) Analysis of the operator splitting scheme for the Allen–Cahn equation, Numerical Heat Transfer, Part B: Fundamentals, 70:5, 472–483, DOI: [10.1080/10407790.2016.1215714](https://doi.org/10.1080/10407790.2016.1215714)

To link to this article: <https://doi.org/10.1080/10407790.2016.1215714>



Published online: 26 Sep 2016.



Submit your article to this journal [↗](#)



Article views: 208



View related articles [↗](#)



View Crossmark data [↗](#)



Citing articles: 6 View citing articles [↗](#)

Analysis of the operator splitting scheme for the Allen–Cahn equation

Zhifeng Weng and Longkun Tang

School of Mathematics Science, Huaqiao University, Quanzhou, P.R. China

ABSTRACT

This paper presents two numerical schemes for solving the Allen–Cahn equation representing a model for antiphase domain coarsening in a binary mixture. Based on the operator splitting method, the Allen–Cahn equation was divided into a linear and a nonlinear sub equation: the linear sub equation was solved by a Fourier spectral method, which is based on the exact solution and thus has no stability restriction on the time-step size; the nonlinear sub equation was then solved analytically due to the availability of a closed-form solution. The stability and error analysis of the numerical solution are presented in detail. Numerical experiments are presented to confirm the accuracy, efficiency, and stability of the proposed method. In particular, we show that the schemes are unconditionally stable and second-order accurate in time.

ARTICLE HISTORY

Received 18 March 2016

Accepted 23 June 2016

1. Introduction

The Allen–Cahn equation is a special type of nonlinear partial differential equation, which arises as reaction–diffusion problems in material science or convection–diffusion equations in computational fluid dynamics. These equations are originally used to solve the phase transition problems, transformation of a thermodynamic system from one phase to another due to an abrupt change in one or more physical properties.



In this paper, we focus on the following Allen–Cahn equation

$$\begin{cases} \frac{\partial u(\mathbf{x}, t)}{\partial t} = \Delta u(\mathbf{x}, t) - \frac{1}{\varepsilon^2} F'(u), & (\mathbf{x}, t) \in \Omega \times (0, T], \\ u(\mathbf{x}, 0) = u^0(\mathbf{x}), & \mathbf{x} \in \Omega. \end{cases} \quad (1)$$

equipped with the homogeneous Neumann boundary condition

$$\nabla u(\mathbf{x}) \cdot n_\Omega = 0, \quad \mathbf{x} \in \partial\Omega. \quad (2)$$

Here, Ω is a bounded domain in $R^d (d = 1, 2, 3)$ and n_Ω denotes the normal vector on $\partial\Omega$. The solution u is defined as the difference between the concentrations of the two components in a mixture (e.g., $u = \frac{m_\alpha - m_\beta}{m_\alpha + m_\beta}$ where m_α and m_β are the mole fractions of phases α and β). The variable u is also known as the order parameter, which represents the local state of the entire system. For example, $u = 1$ in the one phase and $u = -1$ in the other phase. The interface between two phases is defined by $\Gamma_t = \{\mathbf{x} | u(\mathbf{x}, t) = 0\}$ at time t . The function $F(u) = \frac{1}{4}(u^2 - 1)^2$ is the Helmholtz free energy density, which has a double-well form. And we write $F'(u)$ to indicate the derivative of $F(u)$ with respect to u . The small positive constant ε is the gradient energy coefficient related to the interfacial energy.

CONTACT Zhifeng Weng  zfwmath@163.com  School of Mathematics Science, Huaqiao University, Quanzhou 362021, P.R. China

Color versions of one or more of the figures in the article can be found online at www.tandfonline.com/unhb.

© 2016 Taylor & Francis

The Allen–Cahn equation can be derived as the L^2 -gradient flow of the total free energy. This equation is of interest in material science, describing the motion of anti phase boundaries in crystalline solids [1]. Recently, it has been applied to a wide range of problems such as the motion by mean curvature flows [2–5], crystal growth [6, 7], image analysis [8, 9], and two-phase fluid flows [10]. In particular, it has become a basic model equation for the diffuse interface approach developed to study phase transitions and interfacial dynamics in material science [11]. However, the exact solution of the phase-field models can not be found. Therefore, it is very important to develop efficient and highly accurate numerical methods for the Allen–Cahn equation to better understand its dynamics.

Various numerical methods have been developed to solve the Allen–Cahn equation. We refer the readers to [12–14] for finite difference method. To deal with a severe stability restriction on the time step, Eyre [15, 16] proposed a semi-implicit method, which is first-order accurate in time and unconditionally gradient stable. Choi et al. [17] the authors proposed an unconditionally gradient stable scheme to solve the Allen–Cahn equation using Eyre's method. To alleviate the stability constraint and maintain accuracy and simplicity, many researchers used first- and second-order stabilized semi-implicit methods for solving Allen–Cahn equation [19–22]. Yang [20] introduced a stabilized semi-implicit (in time) scheme and a splitting scheme for the equation. Zhang and Du [18] the authors proposed an adaptive finite-element approximation of the the Allen–Cahn equation in the sharp interface limit. A high-order and energy stable scheme was developed to simulate some phase-field models by combining the semi-implicit spectral deferred correction method and the energy stable convex splitting technique [23]. Feng and Li [24] recently presented the analysis for the fully discrete interior penalty discontinuous Galerkin methods for the Allen–Cahn equation.

Alternative methods implemented for solving the Allen–Cahn equation is the operator splitting method [25–27]. The basic idea of the operator splitting method is that the original problem is divided into subproblems which are simpler than the original problem. Then the approximate solution of the original problem is composed using the exact or approximate solutions of the subproblems in a given sequential order. In comparison with semi-implicit schemes, the operator splitting methods are easy to implement and computationally efficient to achieve higher order accuracy. Due to the unconditional stability of each substep, the first- and the second-order operator splitting methods [25–27] are unconditionally stable.

In this paper, we pay close attention to the stability and convergence analysis of the second-order operator splitting method for the Allen–Cahn equation in the two-dimensional case. The Allen–Cahn equation was first divided into linear homogeneous heat equation and nonlinear equation. The linear homogeneous heat equation was solved using Fourier spectral spatial discretization, and the nonlinear part was solved analytically. Then, the stability and error estimate of the operator splitting schemes are discussed in L^2 -norm. The global discrete error is composed of the truncated errors from the splitting, the nonlinear and linear parts, respectively. It is simple to obtain the first two errors directly by the existing numerical theories, so we concentrate on the convergence of the numerical solution to the linear equation. Finally, we present numerical experiments demonstrating numerical properties and the convergence order of the proposed methods.

The outline of the paper is organized as follows. In Section 2, we propose two numerical schemes for Allen–Cahn equation based on operator splitting methods. The stability and error estimate of the proposed fast explicit operator splitting methods are discussed in Section 3. The numerical results confirming the accuracy and efficiency of the both methods are presented in Section 4. Finally, some concluding remarks will be given in Section 5.

2. Two numerical schemes based on second-order operator splitting methods

In this section, two unconditionally stable second-order operator splitting methods are proposed for solving the Allen–Cahn equation. Both methods are based on Fourier spectral method in space discretization and Strang splitting scheme in time discretization. For simplicity, we only consider two-dimensional (2D) case. One-dimensional (1D) and three-dimensional (3D) cases can be

discussed analogously. We introduce a spatial grid Ω_h of size $h = (b - a)/N$, where N is a positive odd integer, and

$$\Omega_h = \left\{ (x_i, y_j) = (a + (i + 0.5)h, a + (j + 0.5)h), 0 \leq i, j < N \right\}$$

is the set of cell centers. Let $u_{ij}^m = u(x_i, y_j, m\tau)$, where $\tau = T/M$ is the time step and M is the total number of time steps.

We first give a definition used in this paper, which is necessary for the derivation and analysis of our numerical methods

Definition 2.1 Suppose the 2D Laplacian $(-\Delta)$ has a complete set of orthonormal eigenfunctions φ_{pq} corresponding to eigenvalues λ_{pq} on the bounded region $[a, b]^2$, i.e., $(-\Delta)\varphi_{pq} = \lambda_{pq}\varphi_{pq}$. Let

$$\mathcal{U} = \left\{ u = \sum_{p=-\infty}^{\infty} \sum_{q=-\infty}^{\infty} \hat{u}_{pq} \varphi_{pq}, \quad \hat{u}_{pq} = \langle u, \varphi_{pq} \rangle, \quad \sum_{p=-\infty}^{\infty} \sum_{q=-\infty}^{\infty} (|\hat{u}_{pq}|^2 |\lambda_{pq}|) < \infty, \right\},$$

Then for any $u \in \mathcal{U}$, it is easy to have

$$(-\Delta)u = \sum_{p=-\infty}^{\infty} \sum_{q=-\infty}^{\infty} \lambda_{pq} \hat{u}_{pq} \varphi_{pq}, \quad (3)$$

where λ_{pq} and φ_{pq} are given by

$$\begin{cases} \lambda_{pq} = 0, & \varphi_{pq} = 0, & \forall p, q < 0, \\ \lambda_{pq} = \left(\frac{\pi p}{b-a}\right)^2 + \left(\frac{\pi q}{b-a}\right)^2, & & \forall p, q \geq 0, \\ \varphi_{pq} = \frac{2}{b-a} \cos\left(\frac{\pi p(x-a)}{b-a}\right) \cos\left(\frac{\pi q(y-a)}{b-a}\right), & & \forall p, q \geq 0, \\ \hat{u}_{pq}(t) = \frac{1}{C_p C_q} \int_{\Omega} u \varphi_{pq} d\mathbf{x}, & & \forall p, q \geq 0. \end{cases} \quad (4)$$

where C_p and C_q are defined as

$$C_r = \begin{cases} 2, & r = 0, \\ 1, & r > 0. \end{cases}$$

Then in virtue of the theory of spectral method [28], we use the Fast Fourier Transformation (FFT) algorithm to compute the discrete Fourier coefficients $\{\hat{u}_{pq}(t)\}$ from the point values $\{u_{ij}(t)\}$ and approximate $\{u_{ij}(t)\}$ by its Fourier expansion:

$$\begin{aligned} \hat{u}_{pq}(t) &= \frac{h^2}{C_p^* C_q^*} \sum_{i=0}^{N-1} \sum_{j=0}^{N-1} u_{ij}(t) \varphi_{pq}(x_i, y_j), \\ u_{ij}(t) &= \sum_{p=0}^{N-1} \sum_{q=0}^{N-1} \hat{u}_{pq}(t) \varphi_{pq}(x_i, y_j), \end{aligned} \quad (5)$$

where C_p^* and C_q^* are, respectively, defined as

$$C_r^* = \begin{cases} 2, & \text{mod}(r, N) = 0, \\ 1, & \text{otherwise.} \end{cases}$$

Now, we use an operator splitting method to split the original problem (1), which can be briefly described as follows. We first denote by S^A and S^B the exact solution operators associated with the heat equation

$$u_t = \Delta u \quad (6)$$

and the nonlinear equation

$$u_t = -\frac{1}{\epsilon^2} f(u). \quad (7)$$

Therefore, the solution of problem (1) can be evolved in time in three substeps:

$$u^{m+1} = \mathcal{S}^A\left(\frac{\tau}{2}\right) \mathcal{S}^B(\tau) \mathcal{S}^A\left(\frac{\tau}{2}\right) u^m, \quad (8)$$

or

$$u^{m+1} = \mathcal{S}^B\left(\frac{\tau}{2}\right) \mathcal{S}^A(\tau) \mathcal{S}^B\left(\frac{\tau}{2}\right) u^m. \quad (9)$$

This three-step splitting algorithm is second-order accurate based on the Strang operator splitting scheme [29]. Higher order splitting schemes can be found in [30, 31]. Next the exact solution operators \mathcal{S}^A and \mathcal{S}^B are replaced by their numerical approximations \mathcal{S}_h^A and \mathcal{S}_h^B .

First, we have the (pq) -th Fourier mode of Eq. (6) from Eq. (3)

$$\frac{\partial \hat{u}_{pq}}{\partial t} = -\lambda_{pq} \hat{u}_{pq}. \quad (10)$$

Second, Eq. (10) is solved analytically with an initial condition \hat{u}_{pq}^m by the method of separation of variables [32].

$$\hat{u}_{pq}^{m+1} = e^{-\lambda_{pq}\tau} \hat{u}_{pq}^m, \quad (11)$$

Hence, we have

$$\mathcal{S}_h^A : u^{m+1} = \mathcal{F}^{-1} [e^{-\lambda_{pq}\tau} \mathcal{F}[u^m](p, q)],$$

where \mathcal{F} denotes the discrete cosine transform and \mathcal{F}^{-1} is inverse.

Then Eq. (7) can be solved analytically whose solution is given as following [25]:

$$\mathcal{S}_h^B : u^{m+1} = \frac{u^m}{\sqrt{e^{-2\tau/\epsilon^2} + (u^m)^2 (1 - e^{-2\tau/\epsilon^2})}}. \quad (12)$$

In a word, to calculate u^{m+1} from u^m , we have two second-order operator splitting methods as follows:

$$\text{MI} : \begin{cases} u^* = \mathcal{F}^{-1} [e^{-\lambda_{pq}\frac{\tau}{2}} \mathcal{F}[u^m](p, q)], \\ u^{**} = \frac{u^*}{\sqrt{e^{-2\tau/\epsilon^2} + (u^*)^2 (1 - e^{-2\tau/\epsilon^2})}}, \\ u^{m+1} = \mathcal{F}^{-1} [e^{-\lambda_{pq}\frac{\tau}{2}} \mathcal{F}[u^{**}](p, q)]. \end{cases} \quad (13)$$

$$\text{MII} : \begin{cases} u^* = \frac{u^m}{\sqrt{e^{-\tau/\epsilon^2} + (u^m)^2 (1 - e^{-\tau/\epsilon^2})}}, \\ u^{**} = \mathcal{F}^{-1} [e^{-\lambda_{pq}\tau} \mathcal{F}[u^*](p, q)], \\ u^{m+1} = \frac{u^{**}}{\sqrt{e^{-\tau/\epsilon^2} + (u^{**})^2 (1 - e^{-\tau/\epsilon^2})}}. \end{cases} \quad (14)$$

Note that the overall time discretization error of the operator splitting methods only come from the splitting error. For every time step, the local splitting error is $O(\tau^3)$ according to Strang's analysis

[29]. Thus, the time error in the proposed methods is second order, and the spatial discretization is spectral order of accuracy.

3. Stability and error analysis

The stability and error analysis of the methods **MI** and **MII** should be studied to get a reasonable solution. Now we deduce the following stability statement and the corresponding proof is also given.

Theorem 3.1 *The methods **MI** and **MII** are unconditionally stable in the sense that for all $h > 0$ and $\tau > 0$, that is, it holds*

$$\|u^{m+1}\| \leq e^{\frac{\tau}{\epsilon^2}} \|u^0\|,$$

where $\|\cdot\|$ denotes the discrete L^2 -norm.

Proof. For convenience, we only give the proof of the method **MI**, the case of **MII** can be discussed similarly.

Using the Parseval's identity and the fact that $e^{-\lambda_{pq}\tau} < 1 (\forall p, q)$, it follows from the first formula of method **MI** that

$$\|u^*\| = \sqrt{\sum_{p,q=0}^{N-1} |\hat{u}_{pq}^*|^2} = \sqrt{\sum_{p,q=0}^{N-1} |e^{-\lambda_{pq}\tau} \hat{u}_{pq}^m|^2} \leq \sqrt{\sum_{p,q=0}^{N-1} |\hat{u}_{pq}^m|^2} \leq \|u^m\|. \quad (15)$$

Now we discuss the second formula of the method **MI**. Since

$$|(u_{ij}^{**})^2| = \frac{(u_{ij}^*)^2}{e^{-2\tau/\epsilon^2} + (u_{ij}^*)^2 (1 - e^{-2\tau/\epsilon^2})} \leq \frac{(u_{ij}^*)^2}{e^{-2\tau/\epsilon^2}} = e^{2\tau/\epsilon^2} (u_{ij}^*)^2,$$

it follows that

$$\|u^{**}\| \leq e^{\tau/\epsilon^2} \|u^*\|. \quad (16)$$

For last formula of method **MI**, an argument similar to the one used in Eq. (15) shows that

$$\|u^{m+1}\| \leq \|u^{**}\|. \quad (17)$$

Therefore from Eqs. (15)–(17), we obtain expected result:

$$\|u^{m+1}\| \leq e^{\tau/\epsilon^2} \|u^m\| \leq e^{T/\epsilon^2} \|u^0\|, \quad (18)$$

where T is final time. This completes the proof.

Next, we will present the main convergence result. Let us start by introducing some notations and lemmas used in this paper, which are necessary for the derivation and analysis of our numerical method. Moreover, we will restrict ourselves to the method **MI**. For the method **MII**, we can use the similar idea to finish the proof. The details are thus omitted.

In the following, we use C , with or without subscript, to denote a generic positive constant whose value may change from place to place but remains independent of the mesh parameter.

Let $\tilde{u}(x, y, t)$ and U^m denote the exact solution of scheme (8) and the numerical solution at t_m of the operator splitting schemes (13). Next we define a grid function space on Ω_h

$$\mathcal{W}^h = \{U \mid U = \{u_{ij} \mid 0 \leq i, j \leq N-1\}\}.$$

and a mapping $I^h : H_{neu}^2(\Omega) \rightarrow \mathcal{W}_h$ by

$$I^h(u) = U,$$

where $H_{neu}^2(\Omega) = \{u \in H^2(\Omega) \mid \nabla u(\mathbf{x}) \cdot \mathbf{n}_\Omega = 0\}$.

Lemma 3.1 *For any grid function $U \in W^h$, it holds that*

$$\|\mathcal{S}_h^A U\| \leq \|U\|.$$

Proof. The result can be obtained from Theorem 3.1.

Lemma 3.2 *For any grid function $U \in W^h$, it holds that*

$$\|\mathcal{S}_h^B U\| \leq e^{\tau/\epsilon^2} \|U\|.$$

Proof. The result can be obtained from Theorem 3.1.

Lemma 3.3 *For any functions $u_0 \in H_{Neu}^s(\Omega)$ with $s > 1$, it holds that*

$$\|I^h \mathcal{S}_h^A u_0 - \mathcal{S}_h^A I^h u_0\| \leq Ch^s |u_0|_s,$$

where $H_{Neu}^s(\Omega) = \{u \in H^s(\Omega) \mid \nabla u(\mathbf{x}) \cdot \mathbf{n}_\Omega = 0\}$ and $|u|_s = \sum_{p,q=-\infty}^{\infty} \lambda_{pq} \hat{u}_{pq} \Phi_{pq}$.

Proof. The proof is similar to that of Lemma 3.4 in [33] and will be omitted here for convenience.

Next, we will present the main convergence result.

Theorem 3.3 *Suppose that $u^{m+1} \in H_{Neu}^s(\Omega)$ with $s > 1$, and U^{m+1} are the exact solution of Eq. (1) and the numerical solution of the proposed method, respectively. Then, there exists a positive constant C independent on τ and h , such that*

$$\|I^h u^{m+1} - U^{m+1}\| \leq C \left(\tau^2 + \frac{h^s}{\tau} \right).$$

Proof. For $m \geq 0$, we have

$$\|I^h u^{m+1} - U^{m+1}\| \leq \|I^h u^{m+1} - I^h \tilde{u}^{m+1}\| + \|I^h \tilde{u}^{m+1} - U^{m+1}\|.$$

The first term on the left-hand side of the above inequality is bounded by

$$\|I^h \tilde{u}^{m+1} - I^h u^{m+1}\| \leq C_1 \tau^3.$$

Then we consider the second term, by Lemmas 3.1 and 3.3

$$\begin{aligned} & \|I^h \tilde{u}^{m+1} - U^{m+1}\| \\ &= \|I^h \mathcal{S}_h^A \mathcal{S}_h^B \mathcal{S}_h^A \tilde{u}^m - \mathcal{S}_h^A \mathcal{S}_h^B \mathcal{S}_h^A U^m\| \\ &\leq \|I^h \mathcal{S}_h^A \mathcal{S}_h^B \mathcal{S}_h^A \tilde{u}^m - \mathcal{S}_h^A I^h \mathcal{S}_h^B \mathcal{S}_h^A \tilde{u}^m\| + \|\mathcal{S}_h^A I^h \mathcal{S}_h^B \mathcal{S}_h^A \tilde{u}^m - \mathcal{S}_h^A \mathcal{S}_h^B \mathcal{S}_h^A U^m\| \\ &\leq C_2 h^s |\mathcal{S}_h^B \mathcal{S}_h^A \tilde{u}^m|_s + \|I^h \mathcal{S}_h^B \mathcal{S}_h^A \tilde{u}^m - \mathcal{S}_h^B \mathcal{S}_h^A U^m\|. \end{aligned}$$

Due to the fact that S^B is solved analytically, and by the Lemmas 3.2, it follows

$$\begin{aligned} & \|I^h S^B S^A \tilde{u}^m - S_h^B S_h^A U^m\| \\ & \leq \|I^h S^B S^A \tilde{u}^m - S_h^B I^h S^A \tilde{u}^m\| + \|S_h^B I^h S^A \tilde{u}^m - S_h^B S_h^A U^m\| \\ & \leq e^{\tau/\epsilon^2} \|I^h S^A \tilde{u}^m - S_h^A U^m\|. \end{aligned}$$

By the Lemmas 3.1 and 3.3 again, it follows

$$\begin{aligned} & \|I^h S^A \tilde{u}^m - S_h^A U^m\| \\ & \leq \|I^h S^A \tilde{u}^m - S_h^A I^h \tilde{u}^m\| + \|S_h^A I^h \tilde{u}^m - S_h^A U^m\| \\ & \leq C_2 h^s |\tilde{u}^m|_s + \|I^h \tilde{u}^m - U^m\|. \end{aligned}$$

Hence, a combination of the above estimates leads to

$$\begin{aligned} & \|I^h u^{m+1} - U^{m+1}\| \\ & \leq C_1 \tau^3 + C_2 h^s (|\tilde{u}^m|_s + e^{\tau/\epsilon^2} |S^B S^A \tilde{u}^m|_s) + \|I^h u^m - U^m\| \\ & \leq (m+1) \left[C_1 \tau^3 + C_2 h^s \max_{0 \leq l \leq m} (|\tilde{u}^l|_s + e^{\tau/\epsilon^2} |S^B S^A \tilde{u}^l|_s) \right] + e^{\tau/\epsilon^2} \|I^h u^0 - U^0\| \\ & \leq C(\tau^2 + h^s/\tau). \end{aligned}$$

The last step is due to the facts that $e^\tau/\epsilon^2 \leq e^T/\epsilon^2$ and $I^h u^0 = U^0$. This ends the proof. \square

Remark 1 When the Allen–Cahn equation was solved by numerical schemes **MI** and **MII** based on the second-order operator splitting method, the numerical results are almost not affected by the order of operator evaluation. The desired order of accuracy is achieved regardless of operator evaluation order since both S^A and S^B have semi-analytic formulas satisfying semigroup properties.

4. Numerical experiments

In this section, numerical examples are performed to study the convergence order and the stability of both schemes **MI** and **MII** based on the operator splitting method for the Allen–Cahn equation. From the results of these numerical tests, it was confirmed that the proposed schemes are second-order accurate in time and are unconditionally stable.

4.1. A convergence test

To show the convergence order of the proposed methods, we start with the study of the 1D problem on $(-7, 13) \times (0, 1]$ with $\epsilon = 0.03$ and the solution of problem (1) is as follows

$$u(x, t) = \frac{1}{2} \left(1 - \tanh \left(\frac{x - st}{2\sqrt{2}\epsilon} \right) \right),$$

where $s = \frac{3}{\sqrt{2}\epsilon}$.

The computational investigation is concerned with the temporal errors and convergence orders. In this test, we fix $N = 200$. The computational results for different time steps are presented in Table 1. It is observed that both methods yield temporal approximation orders close to 2. Moreover, these results in Table 1 indicate that the method **MII** is more accurate. For instance, in the computed solution with a L^2 -norm, error is around $3.14 \cdot 10^{-6}$ by the **MI** method using $\tau = 1/80$. For the **MII** method, a more accurate approximate solution with a L^2 -norm error around $1.49 \cdot 10^{-6}$ can be computed with $\tau = 1/40$. Similar comparison can be made other data to reach similar conclusions.

Table 1. Convergence rate with different τ for problem 3.1 by both methods.

| | $\tau =$ | $\frac{1}{10}$ | $\frac{1}{20}$ | $\frac{1}{40}$ | $\frac{1}{80}$ | $\frac{1}{160}$ |
|-----|-------------|----------------|----------------|----------------|----------------|-----------------|
| MI | Err $_{L2}$ | $2.00e^{-4}$ | $5.03e^{-5}$ | $1.26e^{-5}$ | $3.14e^{-6}$ | $7.86e^{-7}$ |
| | Rate | – | 1.99 | 2.00 | 2.00 | 2.00 |
| MII | Err $_{L2}$ | $2.54e^{-5}$ | $6.04e^{-6}$ | $1.49e^{-6}$ | $3.70e^{-7}$ | $9.26e^{-8}$ |
| | Rate | – | 2.07 | 2.02 | 2.01 | 2.00 |

4.2. A stability test

Now we show that both methods **MI** and **MII** are unconditionally stable. The second problem with $\varepsilon = 0.1$ is considered in $(-3\pi/2, 3\pi/2)^2 \times (0, 2]$. The initial condition is given by

$$u_0(x, y) = 0.05 \sin(x) \sin(y).$$

We fix $N = 100$, then choose $\tau = 1, 1/25, 1/50, 1/200$, and $1/1000$ for methods **MI** and **MII**, respectively. *Figures 1–3* show the numerical solution contour plots at the $T = 2$ with different time steps and the corresponding cputimes (in seconds) are given. These figures suggest that both methods are indeed unconditionally stable even with large time step $\tau = 1$. Moreover, they also show that the **MII** method can obtain higher accuracy solution than the **MI** method. For instance, the numerical solution obtained by **MII** with $\tau = 1/200$ is the same accurate as $\tau = 1/1000$, as shown *Figure 2(d)* and *Figure 3(b)*. However, for the method **MI**, compared with the result with $\tau = 1/1000$, the solution with $\tau = 1/200$ is far from accurate. Furthermore, it is found that, with the same time size τ , the method **MI** requires almost twice as much time as **MII**. This fact once again reinforces the advantage of the method **MII**.

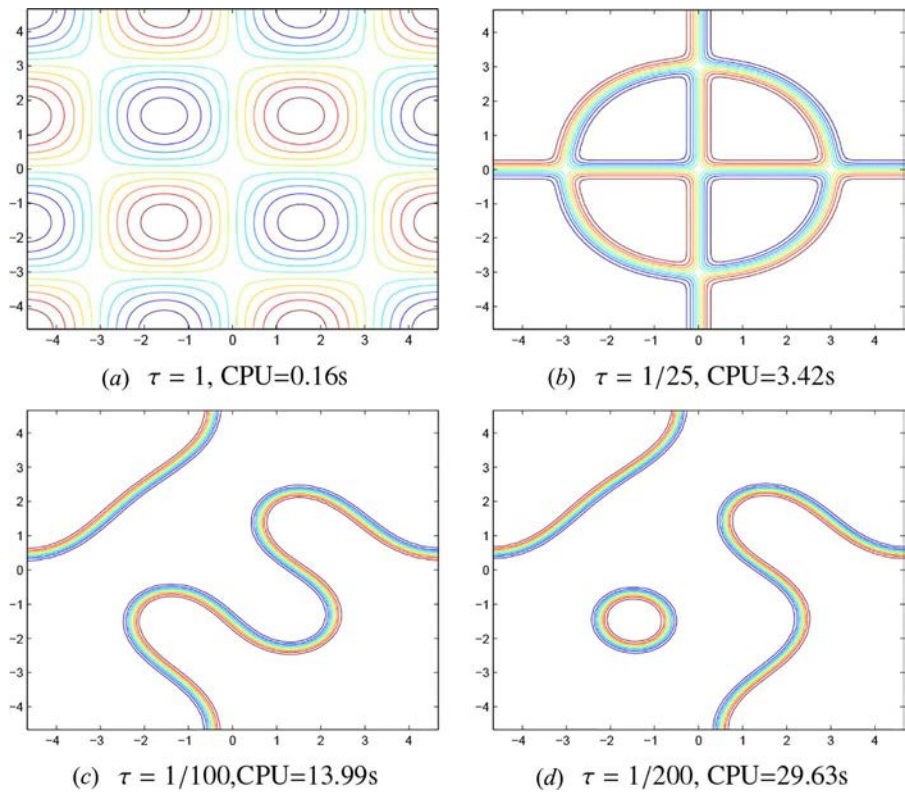


Figure 1. Numerical solution contour plots by method **MI** with different time steps and the corresponding CPU times for problem 4.2.

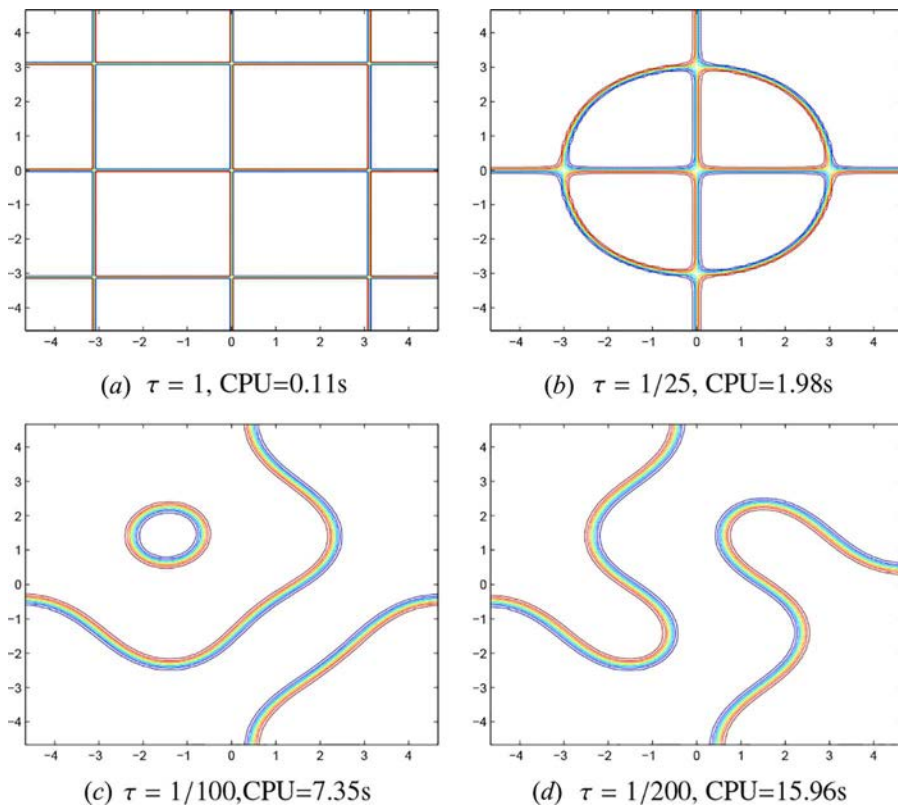


Figure 2. Numerical solution contour plots by method **MI** with different time steps and the corresponding CPU times for problem 4.2.

4.3. 3D case: Randomly perturbed concentration

To further verify the efficiency of the method **MI**, a 3D example is considered in domain $(0, 2)^3 \times (0, 5]$ with $\varepsilon^2 = 0.05$. The initial condition is as follows

$$u_0(x, y, z) = 0.05 \text{ rand}(x, y, z).$$

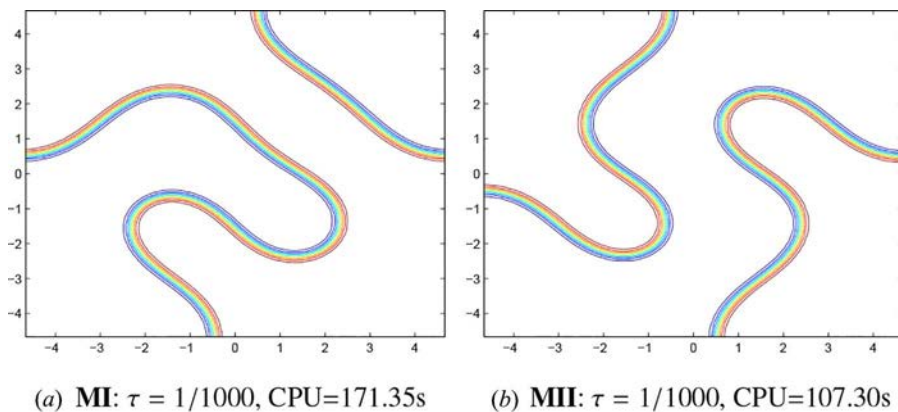


Figure 3. Numerical solution contour plots by both methods with $\tau = 1/1000$ and the corresponding CPU times for problem 4.2.

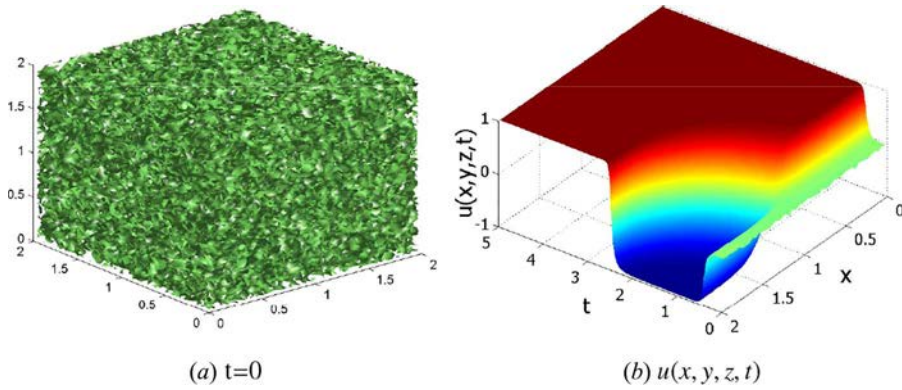


Figure 4. The initial value (a) and the numerical solution with $x = y = z$ by method MII (b) for problem 4.3.

Here, $\text{rand}(x, y, z)$ is a random number between -0.05 and 0.05 . The snapshot of u_0 has been shown in Figure 4(a). In this problem, we fix $h = 1/25$ and $\tau = 1/50$.

Figure 4(b) shows the evolution of the solutions by the method MII as we form the transition layer, metastable state and then reach the stable state, respectively. We see the fast dynamics from the initial condition to the metastable state, where two transition layers are formed.

The morphology evolution results are presented in Figure 5, from which we find that the solution rapidly separates into regions of $u = \pm 1$ (Figure 5(a)), which then evolve over much longer time-scales (Figure 5(b–d)).

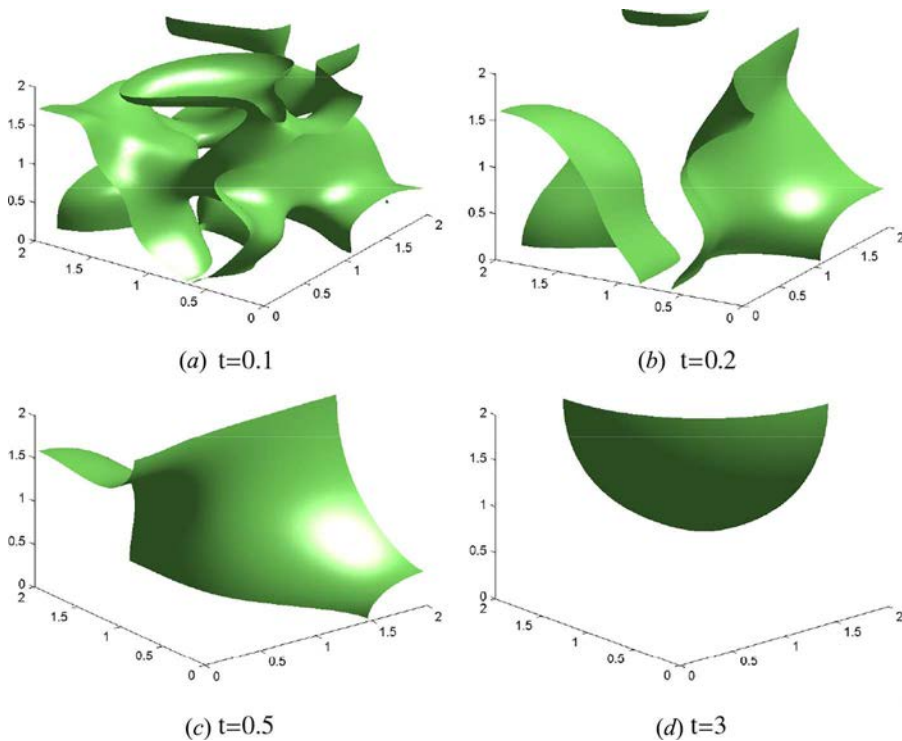


Figure 5. Each shows the surface at the same point in time by method MII for problem 4.3.

5. Conclusions

In this work, by a combination of the operator splitting method and the high accurate Fourier spectral method, two second-order fast operator splitting methods for the Allen–Cahn equation were developed. The stability and error estimate of both schemes were derived. Numerical experiments verified the effectiveness and the accuracy of both schemes. Additionally, during the simulations, it is observed that the method **MII** has competitive advantages both in accuracy and CPU time. In future work, we plan to extend this method to 3D Cahn–Hilliard equation.

Acknowledgements

This work is in part supported by the Scientific Research Foundation of Huaqiao University (No. 15BS307), the Natural Science Foundation of Fujian Province (No. 2016J05007) and Promotion Program for Young and Middle-aged Teacher in Science and Technology Research of Huaqiao University (ZQN-YX301) and the NSF of China (Nos. 11526094 and 61573004). The authors would like to thank the editor and referees for their valuable comments and suggestions which helped us to improve the results of this paper.

References

- [1] S. Allen and J. Cahn, A Microscopic Theory for Antiphase Boundary Motion and its Application to Antiphase Domain Coarsening, *Acta Metall.*, vol. 27, pp. 1085–1095, 1979.
- [2] L. Evans, H. Soner, and P. Souganidis, Phase Transitions and Generalized Motion by Mean Curvature, *Comm. Pure Appl. Math.*, vol. 45, pp. 1097–1123, 1992.
- [3] X. Feng and A. Prohl, Numerical Analysis of the Allen–Cahn equation and Approximation for Mean Curvature Flows, *Numer. Math.*, vol. 94, pp. 33–65, 2003.
- [4] T. Ilmanen, Convergence of the Allen–Cahn equation to Brakke's Motion by Mean Curvature, *J. Diff. Geom.*, vol. 38, pp. 417–461, 1993.
- [5] T. Ohtsuka, Motion of Interfaces by an Allen–Cahn Type equation with Multiple-Well Potentials, *Asymptot. Anal.*, vol. 56, pp. 87–123, 2008.
- [6] A. Wheeler, W. Boettinger, and G. McFadden, Phase-Field Model for Isothermal Phase Transitions in Binary Alloys, *Phys. Rev. A*, vol. 45, pp. 7424–7439, 1992.
- [7] M. Cheng and J. Warren, An Efficient Algorithm for Solving the Phase Field Crystal Model, *J. Comput. Phys.*, vol. 227, pp. 6241–6248, 2008.
- [8] M. Beneš, V. Chalupecký, and K. Mikula, Geometrical Image Segmentation by the Allen–Cahn Equation, *Appl. Numer. Math.*, vol. 51, pp. 187–205, 2004.
- [9] J. Dobrosotskaya and A. Bertozzi, A Wavelet-Laplace Variational Technique for Image Deconvolution and Inpainting, *IEEE Trans. Image Process.*, vol. 17, pp. 657–663, 2008.
- [10] X. Yang, J. Feng, C. Liu, and J. Shen, Numerical Simulations of Jet Pinching-Off and Drop Formation using an Energetic Variational Phase-Field Method, *J. Comput. Phys.*, vol. 218, pp. 417–428, 2006.
- [11] L. Q. Chen, Phase-Field Models for Microstructure Evolution, *Ann. Rev. Mater. Res.*, vol. 32, pp. 113–140, 2002.
- [12] X. Chen, C. Elliott, A. Gardiner, and J. Zhao, Convergence of Numerical Solutions to the Allen–Cahn Equation, *Appl. Anal.*, vol. 69, pp. 47–56, 1998.
- [13] S. Zhai, X. Feng, and Y. He, Numerical Simulation of Three Dimensional Allen–Cahn Equation by High-Order Compact ADI Method, *Comput. Phys. Commun.*, vol. 10, no. 185, pp. 2449–2455, 2014.
- [14] D. Jeong, S. Lee, D. Lee, J. Shin, and J. Kim, Comparison Study of Numerical Methods for Solving the Allen–Cahn Equation, *Comp. Mater. Sci.*, vol. 111, pp. 131–136, 2016.
- [15] D. Eyre An Unconditionally Stable One-Step Scheme for Gradient Systems, <http://www.math.utah.edu/eyre/research/methods/stable.ps>.
- [16] D. Eyre Unconditionally Gradient Stable Time Marching the Cahn–Hilliard Equation, in J. Bullard, R. Kalia, M. Stoneham, L.-Q. Chen (Eds.), *Computational and Mathematical Models of Microstructural Evolution*, pp. 39–46, The Material Research Society, Warrendale, PA, 1998.
- [17] J. Choi, H. Lee, D. Jeong, and J. Kim, An Unconditionally Gradient Stable Numerical Method for Solving the Allen–Cahn Equation. *Physica A*, vol. 388, pp. 1791–1803, 2009.
- [18] J. Zhang and Q. Du, Numerical Studies of Discrete Approximations to the Allen–Cahn Equation in the Sharp Interface Limit, *SIAM J. Sci. Comput.*, vol. 31, pp. 3042–3063, 2009.
- [19] J. Shen and X. Yang, An Efficient Moving Mesh Spectral Method for the Phase-Field Model of Two-Phase Flows, *J. Comput. Phys.*, vol. 228, pp. 2978–2992, 2009.

- [20] X. Yang, Error Analysis of Stabilized Semi-Implicit Method of Allen–Cahn Equation, *Discrete Contin. Dyn. B*, vol. 11, pp. 1057–1070, 2009.
- [21] J. Shen and X. Yang, Numerical Approximations of Allen–Cahn and Cahn–Hilliard Equations, *Discrete Contin. Dyn. A*, vol. 28, pp. 1669–1691, 2010.
- [22] X. Feng, H. Song, T. Tang, and J. Yang, Nonlinear Stability of the Implicit-Explicit Methods for the Allen–Cahn Equation, *Inverse Problems and Imaging (A special issue in honor of Tony Chan’s 60th birthday)*, vol. 7, pp. 679–695, 2013.
- [23] X. Feng, T. Tang, and J. Yang, Long Time Numerical Simulations for Phase-Field Problems Using p-Adaptive Spectral Deferred Correction Methods, *SIAM J. Sci. Comput.*, vol. 37, pp. A271–A294, 2015.
- [24] X. Feng and Y. Li Analysis of interior penalty discontinuous Galerkin methods for the Allen–Cahn Equation and the mean curvature flow, arXiv:1310.7504 (preprint).
- [25] Y. Li, H. Lee, D. Jeong, and J. Kim, An Unconditionally Stable Hybrid Numerical Method for Solving the Allen–Cahn Equation, *Comput. Math. Appl.*, vol. 60, pp. 1591–1606, 2010.
- [26] H. Lee and J. Lee, A Semi-Analytical Fourier Spectral Method for the Allen–Cahn Equation, *Comput. Math. Appl.*, vol. 68, pp. 174–184, 2014.
- [27] H. Lee and J. Lee, A Second Order Operator Splitting Method for Allen–Cahn Type Equations with Nonlinear Source Terms, *Physica A*, vol. 432, pp. 24–34, 2015.
- [28] J. Shen, T. Tang, and L. Wang *Spectral Methods Algorithms: Analyses and Applications*. 1st ed., Springer, Berlin, 2010.
- [29] G. Strang, On the Construction and Comparison of Difference Schemes, *SIAM J. Numer. Anal.*, vol. 5, pp. 506–517, 1968.
- [30] S. Blanes and P. Moan, Practical Symplectic Partitioned Runge–Kutta and Runge–Kutta–Nyström Methods, *J. Comput. Appl. Math.*, vol. 142, no. 2, pp. 313–330, 2002.
- [31] P. Csomós, I. Faragó, and Á. Havasi, Weight Sequential Splitting and their Analysis, *Comput. Math. Appl.*, vol. 50, pp. 1017–1031, 2005.
- [32] A. Stuart and A. Humphries *Dynamical System and Numerical Analysis*. Cambridge University Press, Cambridge, 1998.
- [33] X. Li, Z. Qiao, and Zhang, H. 2015 Convergence of the fast explicit operator splitting method for the molecular beam epitaxy model, arXiv:1506.05271. (arXiv preprint)